# Effect of Atom Substitutions on the Magnetic Properties in $Ce_2Fe_{17}$: Towards Permanent Magnet Applications

Li Yin*, and David S. Parker

*Material Science and Technology Division, Oak Ridge National Laboratory, Oak Ridge, TN 37831, USA*

*Author to whom correspondence should be addressed: yinl@ornl.gov

# ABSTRACT

Due to the rapidly developing technologies and huge market demand, there has been increasing interest internationally in exploring permanent magnet formulations in addition to the well-known $Nd_2Fe_{14}B$ and $SmCo_5/Sm_2Co_{17}$. Given Fe's low materials cost and generally high magnetization, Fe-rich rare earth binaries such as $Ce_2Fe_{17}$ comprise a rich "hunting ground" for such new materials. While this compound suffers from a low ordering point and, is a *heli*magnet, these difficulties are easily remedied by substitution of appropriate amounts of Cobalt for Fe, with room-temperature saturation magnetization as high as 1.5 T. Here we try to switch the all-important magnetic anisotropy from planar to uniaxial behavior in $Ce_2Fe_{17}$ via 18*h*- and 6*c*-type atom substitutions with Si, Ir and numerous other atoms. The uniaxial magnetocrystalline anisotropy is successfully achieved in the 6*c*-site-substitued $Ce_2Fe_{15}Ir_2$ systems, along with large magnetization. We find the iridium substitution, in particular, induces a substantial uniaxial anisotropy of 11.25 $MJ/m^3$, which is comparable to most of the current rare earth permanent magnets. Although the iridium substitution is costly, the finding of Ir-triggered uniaxial magnetic anisotropy indicates the potential of Ce-Fe-based alloys for permanent magnets.

# I. INTRODUCTION

In past decades, permanent magnets[1,2] have been intensively studied due to their increasing technological importance in applications such as traction motors and electrical generators. In general, high performance permanent magnets require a difficult-to-achieve combination of uniaxial magnetic anisotropy, thermal stability, high Curie temperature (usually exceeding 500 K) and a large value of the saturation magnetization. Relatively few materials meet all these requirements.[1] In addition, state-of-the-art permanent magnets often contain the critical elements Nd or Dy, which are subject to supply disruptions.[2] Considering the rapidly developing technologies and huge market demand, it is of considerable importance to explore critical-element-free permanent magnet formulations. Owing to the localized nature of *f* electrons,[3] rare earth elements are highly favorable to achieving excellent magnetic properties in permanent magnets. In particular, Ce is the most common of the lanthanides, and Fe is a common inexpensive element usually producing a large magnetic moment. So, an Fe-rich compound containing Ce is a natural starting place to explore critical-element-free permanent magnets.

Potential permanent magnet materials with Ce and Fe atoms[1,4] include $CeFe_{11}Ti$, $CeFe_5$, $Ce_2Fe_{14}B$ and $Ce_2Fe_{17}$. None of these compounds meets all the desired permanent magnetic properties. Here, we focus on $Ce_2Fe_{17}$, which shows a strong magnetization when alloyed with elements such as Co to transform its *heli*magnetism to the desired ferromagnetic behavior.[5-7] While, the planar magnetocrystalline anisotropy and low Curie temperature make $Ce_2Fe_{17}$ unfavorable for excellent permanent magnets. However, the Curie temperature and magnetocrystalline anisotropy of $R_2Fe_{17}$ magnets (R=rare earth)[8] are often tunable by

inserting the interstitial light elements[9,10] or employing atom substitutions,[7,11-13] which provide opportunities for achieving high-performance magnet properties. In particular, the interstitial light elements in $R_2Fe_{17}$ known to yield compound formation include C and N. In $Sm_2Fe_{17}$, inserting the C or N atoms can tune the magnetocrystalline anisotropy from planar to uniaxial.[9,10,14] However, this favorable anisotropy behavior does not occur in pure $Ce_2Fe_{17}$. So, in this work, we try to induce the uniaxial magnetic anisotropy and improve the Curie point in $Ce_2Fe_{17}$ by atom substitutions.

In previous studies, various atoms have been studied in $Ce_2Fe_{17}$, such as the Al, Si and Ga.[13] The Curie point of 238 K in $Ce_2Fe_{17}$ is improved to ~460 K in $Ce_2Fe_{14}Si_3$,[7] where the introduced Si atoms generally prefer to occupy the 18*h* sites.[7,15] However, the first anisotropy constant $K_1$ of $Ce_2Fe_{14}Si_3$ remains planar at -0.90 MJ/m$^3$,[16,17] which is disadvantageous for the permanent magnet. The Curie point of $Ce_2Fe_{17}$ can also be improved by Ga substitutions,[13] where the introduced Ga atoms also prefer to occupy the 18*h* site. In $Gd_2Fe_{17-x}Ga_x$, the Curie point increases from $x$=0 to $x$=3, but decreases from $x$=3 to $x$=7. Moreover, the easy magnetization direction in $Gd_2Fe_{17-x}Ga_x$ varies from the basal plane to *c* axis with the increased content of Ga. These results hint at the possibility of attaining uniaxial magnetocrystalline anisotropy in $Ce_2Fe_{17}$ by atom substitutions. So, we investigate the magnetic properties of $Ce_2Fe_{17}$ with Ga substitution in this work. Moreover, both $Ce_2Fe_{17}$ and $Gd_2Fe_{17}$ show the $Th_2Zn_{17}$-type structure. Since the Curie point in $Gd_2Fe_{17-x}Ga$ is highest at $x$=3, we choose the content of $Ce_2Fe_{14}Ga_3$. Meanwhile, other elements with the outermost electron of 4*p*, including Zn, Ge, As and Se, also are studied in this work, in an attempt to create the desired uniaxial magnetic anisotropy in $Ce_2Fe_{17}$.

Before describing our results, we discuss some preliminary structural considerations – the site preferences of the substitutions. In $R_2Fe_{17}$, the 6*c* or 18*h* sites are determined as the main preference sites as the new atoms substitute for Fe.[18] So, except the 18*h*-type Si or Ga substitution, we also consider the 6*c*-type atom substation in this work. In previous studies, Ta, W or Mo atoms show a strong preference for 6*c* site in $R_2Fe_{17}$ with the $Th_2Zn_{17}$-type structure.[12,18-20] Here, we choose W to modify the magnetic properties in $Ce_2Fe_{17}$ by atom substitutions, to compare with the 18*h*-site-prefered Ga case. Moreover, the rare-earth elements are frequently applied in high performance magnet owing to the strong spin-orbit coupling (SOC) caused by *f* electrons. However, SOC is often taken to scale approximately as $Z^4$ (Z denotes the atomic number),[21-23] and the rare earth elements are hardly unique as a source of strong SOC. Introducing other atoms with strong SOC in $Ce_2Fe_{17}$ may modify the magnetocrystalline anisotropy. So, in addition to the 18*h*-site-prefered Ga and 6*c*-site-prefered W substitution, the heavy Ir atom[24,25] is also studied in $Ce_2Fe_{17}$.

In this paper, we investigate the magnetic properties of $Ce_2Fe_{17}$ with 18*h*- and 6*c*-type atom substitutions respectively. The atoms of Si, Zn, Ga, Ge, As and Se preferentially occupy the 18*h* site, and atoms of W and Ir preferentially occupy the 6*c* site. It is found that, the substituted $Ce_2Fe_{17}$ with Si, Zn, Ga, Ge, As, Se or W atom shows the planar magnetocrystalline anisotropy, where the calculated planar magnetic anisotropy of Si case is in agreement with experiments. In particular, the uniaxial magnetocrystalline anisotropy is successfully achieved in the 6*c*-site-substitued $Ce_2Fe_{15}Ir_2$ systems, along with the strong magnetization. We do find an ultrahigh anisotropy of 11.25 $MJ/m^3$ in $Ce_2Fe_{15}Ir_2$, which is comparable to most of the current rare earth permanent magnets. These results provide

substantial insights into developing critical-element-free permanent magnet materials.

# II. METHODS

The first-principles calculations are performed in Vienna Ab initio Simulation Package[26,27] and the all-electron-density functional code WIEN2k.[28,29] The Perdew-Burke-Ernzerhof flavor of spin-polarized generalized gradient approximation (GGA) is applied in all of the calculations.[30] The structures of $Ce_2Fe_{17}$ with different atom substitutions are fully relaxed in Vienna Ab initio Simulation Package, with the projector augment wave pseudo-potentials.[31,32] The plane-wave energy cutoff is 520 eV. The Brillouin Zone is sampled with Γ-centered 4×4×4 $k$ point meshes for relaxing the $Ce_2Fe_{17}$ with different atom substitutions. The convergence criteria for energy and atomic forces are set to $10^{-6}$ eV and 0.005 eV/Å, respectively. The relaxed lattice constants of $Ce_2Fe_{17}$ are $a$=$b$=8.445 Å, $c$=12.610 Å with the volume of 778.885 Å$^3$, which is close to the experimental value of 776.140 Å$^3$.[33] These calculation parameters are used to relax the structures of $Ce_2Fe_{14}M_3$ ($M$=Zn, Ga, Ge, As or Se), $Ce_2Fe_{15}W_2$ and $Ce_2Fe_{15}Ir_2$ shown in Fig. 1. The crystal structure visualization is performed using VESTA 3.4.7.[34]

The calculations of magnetic properties are performed in WIEN2k. The linearized augmented plane wave method[35] is employed. A $RK_{\max}$ of 9.0 is used for good convergence. The charge convergence criterion is set to be 0.0001 electron charge. The magnetocrystalline anisotropy energy (MAE) is calculated with SOC, based on the assumed collinear spin arrangement. MAE is defined as $\left(E_a - E_c\right)/V$, where $E_a$ and $E_c$ are the total energies of the system for the magnetization oriented along the planar $a$ ($[1\,\bar{1}0]$ in a rhombohedral primitive cell) and $c$ ([111] in a rhombohedral primitive cell) directions respectively, $V$ indicates the

volume of the primitive cell. The positive (negative) value of MAE represents the uniaxial (planar) magnetocrystalline anisotropy. MAE is a small quantity in the order of meV/f.u., which can depend rather sensitively on the number of **k** points. So, we have carefully tested **k** point convergence to calculate the MAE in $Ce_2Fe_{17}$ with experimental lattice constants ($a$=$b$=8.496 Å, $c$=12.415 Å, $\alpha$=$\beta$=90°, $\gamma$=120°),[33] where the internal atomic coordinates are relaxed until forces are less than 1 mRy/bohr. As shown in Fig. 2(a), the calculated MAE values at different **k** points are very close. The difference of MAE values at 2000 and 5000 **k** points is 2.6%, and the MAE difference at 2000 and 4000 **k** points is 0.17%. All the MAE results reported here use 2000 **k** points (in the full Brillouin zone).

In addition, the Hubbard $U$ correction has been studied in $Ce_2Fe_{17}$. As shown in Fig. 2(b), different $U$ values have been applied in the Ce 4$f$ electrons to calculate the MAE in $Ce_2Fe_{17}$. It is found that the employed $U$ effect changes the electronic structure of $Ce_2Fe_{17}$ in the vicinity of Fermi level, as shown in Fig. 2(c). As compared with the generalized-gradient approximation (GGA) plus SOC case, both the conduction- and valence-band states move towards the Fermi level with the GGA+SOC+$U$, where the conduction and valence bands are mainly contributed by the Ce 4$f$ and Fe 3$d$ respectively. Such a phenomenon occurs in all the GGA+SOC+$U$ cases. More importantly, in Fig. 2(b), the calculated MAE monotonically increases as the value of $U$ is increased. The calculated MAE of $Ce_2Fe_{17}$ at $U$=0 is -1.90 MJ/m$^3$, which is close to the experimental value[5,36,37] of ~2.2 MJ/m$^3$. So, the applied $U$ appears to exaggerate the MAE in $Ce_2Fe_{17}$. Besides, the valence state of Ce is generally revealed by the density of states in the $f$ electrons. The $f$ states occupying above the Fermi level indicates the trivalent Ce, and $f$ states occupying below the Fermi level denotes the

tetravalent Ce. In $Ce_2Fe_{17}$, as show in Fig. 2(c), although most the f states occupy above the Fermi level, some of the f states are located below the Fermi level. Such phenomenon implies the mixed trivalent or tetravalent Ce, which is consistent with the X-ray absorption spectroscopy demonstrated mixed valent of Ce in $Ce_2Fe_{17}$.[20,38] In addition, referring to Ir-included materials,[39,40] we have tested the Hubbard *U* of 1.0 eV, 1.5 eV and 2.0 eV for Ir 5*d* electrons in $Ce_2Fe_{15}Ir_2$. The calculated MAE and magnetization $Ce_2Fe_{15}Ir_2$ at *U* of 1.0 eV, 1.5 eV or 2.0 eV in Ir 5*d* electrons are larger than the values at *U* of 0.0 eV. The maximum difference of MAE calculated with and without the Hubbard *U* is 4.03%. In this work, the GGA+SOC without Hubbard *U* correction is employed to calculate the MAE in $Ce_2Fe_{17}$ systems with atom substitutions.

# III. RESULTS AND DISCUSSION

$Ce_2Fe_{17}$ shows the rhombohedral $Th_2Zn_{17}$ structure in the space group of R-3m H (166), where the newly introduced atoms could occupy the 6*c*, 9*d*, 18*f* or 18*h* sites to substitute Fe atoms. Especially, in $Ce_2Fe_{17}$, Fe atoms in 6*c* site (i.e., Fe-6*c*) have the smallest number of Ce and the largest number of Fe nearest neighbors. While, Fe atoms in 18*h* site (i.e., Fe-18*h*) have the smallest number of Fe and the largest number of Ce nearest neighbors. In the following, similar to the Fe-6*c* and Fe-18*h*, Fe-9*d* and Fe-18*f* denotes the Fe atoms in 9*d* and 18*f* sites respectively in this work. These Fe atoms in different sites are displayed in Fig. 1. In order to determine the preference sites, total energies of $Ce_2Fe_{15}X_2$ are calculated as the *X* atoms occupy the four sites respectively. Note that the concentration of Fe atoms in 6*c*, 9*d*, 18*f* and 18*h* sites are 2:3:6:6 in $Ce_2Fe_{17}$, where the highest concentration of Fe-6*c* is 2/17. So, the configuration of $Ce_2Fe_{15}X_2$ is used to determine the site preference. As shown in Fig. 3(a),

the introduced Zn and Ga atoms prefer to occupy the 18*h* site, and the W and Ir atoms prefer to occupy the 6*c* site. We have assumed that the Ge, As and Se atoms would also prefer to occupy the 18*h* site in $Ce_2Fe_{17}$, as with the Zn and Ga cases. The corresponding volumes of these substituted $Ce_2Fe_{17}$ compounds are shown in Fig. 3(b).

For the 6*c*-type substitution, the atomic configurations of $Ce_2Fe_{15}W_2$ and $Ce_2Fe_{15}Ir_2$ are used in this work, along with the same symmetries with $Ce_2Fe_{17}$. For the 18*h*-type substitution, the atomic configuration of $Ce_2Fe_{14}M_3$ (*M*=Zn, Ga, Ge, As or Se) is chosen for possible high Curie point.[7,11,13] Meanwhile, the symmetry of $Ce_2Fe_{17}$ in 166 space group can be only minimally lowered in $Ce_2Fe_{14}M_3$ to the 160 space group, where half of the 18*h* Fe atoms, 3/6, are substituted by *M* in $Ce_2Fe_{14}M_3$. Base on such kind of substitution, the symmetry is minimally lowered, where large k points could be used for getting a reliable MAE value. Although in a slightly lower-symmetry structure, the 160 space group maintains the rhombohedral symmetry, which is critical for achieving an accurate MAE value. This avoids spurious results arising from, for example, the assumption of orthorhombic or monoclinic symmetry not present in the experimental system. These results arise due to the lack of equivalence of the planar magnetization directions in these lower symmetry structures, inducing an inaccurate planar variation in magnetic anisotropy. The geometry of $Ce_2Fe_{14}M_3$ is shown in Fig. 1. However, the MAE of $Ce_2Fe_{14}M_3$ (*M*=Zn, Ga, Ge, As or Se) has not been reported in previous experiments. So, the $Ce_2Fe_{14}M_3$ model we have constructed, as shown in Fig. 1, is tested in the Si system. The calculated MAE of $Ce_2Fe_{14}Si_3$ is -0.97 MJ/m$^3$, which is very close to the reported experimental value[16,17] of -0.90 MJ/m$^3$. We have analyzed the magnetocrystalline anisotropy of $Ce_2Fe_{14}Si_3$ with 10%, 20%, 30% and 40% substitutions of

Fe by Co, which is displayed in Fig. 2(d). We find that although the uniaxial magnetocrystalline anisotropy occurs in the 20% case, the achieved value of 0.19 MJ/m$^3$ is too small to be used in permanent magnets. Next, we use this $Ce_2Fe_{14}M_3$ model to investigate the magnetic properties of $Ce_2Fe_{17}$ with Zn, Ga, Ge, As or Se substitutions.

Magnetocrystalline anisotropy, magnetization and Curie temperature are three indispensable properties for a permanent magnetic material. Here, we analyze the anisotropy and magnetization in $Ce_2Fe_{14}M_3$, $Ce_2Fe_{15}W_2$ and $Ce_2Fe_{15}Ir_2$. In $Ce_2Fe_{15}W_2$, the MAE increases in magnitude as compared with the calculated MAE in $Ce_2Fe_{17}$, but remains planar at -3.23 MJ/m$^3$. The magnetization in $Ce_2Fe_{15}W_2$ decreases to 1.24 T, which is substantially smaller than the value of 1.72 T in $Ce_2Fe_{17}$. Both the planar anisotropy and reduced magnetization make $Ce_2Fe_{15}W_2$ unfavorable for permanent magnets. The magnetocrystalline anisotropy and magnetization in $Ce_2Fe_{14}M_3$ and $Ce_2Fe_{15}Ir_2$ are summarized in Figs. 3(c) and 3(d). It can be found that, the substituted $Ce_2Fe_{17}$ with Zn, Ga, Ge, As or Se atom shows the planar magnetocrystalline anisotropy. In previous experiments, $Ce_2Fe_{17-x}Ga_x.(x \leq 2)$ show the planar magnetic anisotropy.[41] In Fig. 3(c), the magnetic anisotropy in $Ce_2Fe_{14}Ga_3$ still is planar.

However, $Ce_2Fe_{15}Ir_2$ shows the uniaxial magnetocrystalline anisotropy as shown in Fig. 3(c), which is desired in permanent magnets. In particular, the uniaxial MAE of $Ce_2Fe_{15}Ir_2$ is as high as 11.25 MJ/m$^3$, which is more than double that of the excellent permanent magnet $Nd_2Fe_{14}B$ in room temperature. The calculated MAE of 11.25 MJ/m$^3$ of $Ce_2Fe_{15}Ir_2$ is also close to the half of the anisotropy constant (24 MJ/m$^3$) in $Pr_2Fe_{14}B$ in the ultralow temperature of 4.2 K.[42] Here, the planar magnetocrystalline anisotropy in $Ce_2Fe_{17}$ is

transferred to be uniaxial via the Ir substitution in the dumbbell 6*c* site. Such phenomenon is similar to the substituted $Ce_2Co_{17}$, where Co atoms on the dumbbell sites has very negative contributions to the uniaxial MAE, and replacing them with other atoms can generally enhance the uniaxial MAE.[43]

In Fig. 3(d), the magnetization in $Ce_2Fe_{15}Ir_2$ decreases as compared with $Ce_2Fe_{17}$. However, the decreased magnetization in $Ce_2Fe_{15}Ir_2$ is above 1.4 T, which is a substantial value in permanent magnets. The spin and orbital moments of each atom in $Ce_2Fe_{15}Ir_2$ are listed in Table I. We further analyze the DOS in $Ce_2Fe_{15}Ir_2$ system, as shown in Fig. 4. As compared with $Ce_2Fe_{17}$, the total DOS in $Ce_2Fe_{15}Ir_2$ system varies evidently in the energy region far from the Fermi level ($E_F$). In the energy window of [$E_F$-0.6 eV, $E_F$-0.4 eV], the total DOS shows a significant enhancement, which is mainly contributed by the *d* electrons in Ir atom, as shown in Figs. 4(a) and 4(b). Here, the occupation of *d* state in Ir atom is substantially larger than the *p* state. In the *d*-projected partial DOS in Ir atom, the contribution from $m$=±1 ($d_{xz}$ and $d_{yz}$) states is similar to that from $m$=±2 ($d_{xy}$ and $d_{x^2-y^2}$) states, especially near the Fermi level as shown in Fig. 4(b). However, the $m$=0 ($d_{z^2}$) state in Ir atom is obviously different from the $m$=±1 and $m$=±2 states. The distinct $m$=0 state along with the comparable $m$=±1 and $m$=±2 in Ir atom and substantially increased occupied states in $Ce_2Fe_{15}Ir_2$ probably lay the foundation for creating the uniaxial magnetocrystalline anisotropy.

Next, we analyze the Curie point in $Ce_2Fe_{15}Ir_2$ model. Based on the mean-field theory and Heisenberg model,[44,45] the Curie temperature $T_C$ is estimated by the formula $k_BT_C=(E_{FI}-E_{FM})/3$, where $E_{FI}$ and $E_{FM}$ indicate the total energies of system in the

ferrimagnetic and ferromagnetic orders. In this work, three kinds of ferrimagnetic configurations are considered in $Ce_2Fe_{17}$-based systems, as shown in Figs. 5(a)-(d). The Curie point of $Ce_2Fe_{17}$ is firstly calculated based on the three kinds of ferrimagnetic configurations respectively. Note that, generally speaking, one should compare the energetics of the FM configuration with a nearest-neighbor antiferromagnetic state, but the geometric frustration associated with the rhombohedral structure forbids such a comparison. As shown in Fig. 5(e), the calculated Curie points in $Ce_2Fe_{17}$ based on the FI-order1 and FI-order3 are lower and higher than the experimental value of 238 K, respectively. While, the FI-order2 will obviously underestimates the Curie point in $Ce_2Fe_{17}$. So, we use the ferrimagnetic configurations of FI-order1 and FI-order3 to estimate the Curie point of $Ce_2Fe_{15}Ir_2$, and get the value of 263 K and 427 K respectively. Referring to the $Ce_2Fe_{17}$ system, the actual Curie point of $Ce_2Fe_{15}Ir_2$ should be between 263 K and 427 K. Considering that partial substitution of Fe by Co can improve the Curie point in $R_2Fe_{17}$,[46] we have tried to improve the Curie point of $Ce_2Fe_{15}Ir_2$ via substitution of 20% of Fe by Co. However, the ferrimagnetic order in the $Ce_2(Fe_{0.8}Co_{0.2})_{15}Ir_2$ is finally relaxed back to the ferromagnetic order, apparently due to an itinerant magnetism characteristic. Combining the large uniaxial magnetocrystalline anisotropy and relatively large magnetization in $Ce_2Fe_{15}Ir_2$, more studies for improving the Curie point in $Ce_2Fe_{15}Ir_2$ will be of interest in further research.

We also calculate the formation enthaply for the promising $Ce_2Fe_{15}Ir_2$ system. The formation enthalpy of $Ce_2Fe_{15}Ir_2$ is calculated based on its elementary substances. The system with a lower value of formation energy will be thermodynamically more stable. The energies of Ce, Fe and Ir are calculated from their stable phases in Materials Project data base.[47-49] The

calculated formation enthalpy of $Ce_2Fe_{15}Ir_2$ is -0.042 eV/atom, which is negative and lower than the formation enthalpies of pristine $Ce_2Fe_{17}$, $CeFe_5$ and $CeFe_2$ as listed in Table II. By way of comparison, we listed the formation enthalpies of other $R_2Fe_{17}$ compounds in Table II, which are isostructural to $Ce_2Fe_{17}$. It can be found that all the listed $R_2Fe_{17}$ compounds show the higher formation enthalpy than that in $Ce_2Fe_{15}Ir_2$. These results imply the potential formation of $Ce_2Fe_{15}Ir_2$ in experiments.

Furthermore, we analyze the thermodynamic stability and assess the potential decomposition of $Ce_2Fe_{15}Ir_2$ by the grand-canonical linear programming method.[50,51] Considering the ternary phase diagram of $Ce_2Fe_{15}Ir_2$, we examine the Materials Project database, and find several possible decomposition phases, which are summarized in Table II. Owing to the higher formation enthalpies of $CeFe_5$ and $CeFe_2$ than $Ce_2Fe_{15}Ir_2$, their corresponding decomposition pathways are energetically blocked. The possible decomposition pathways are concentrated on the $CeIr_2$, $CeIr_3$, $CeIr_5$ and $FeIr_3$ binary phases. However, the $CeIr_5$ is able to decompose to $CeIr_3$ and Ir, so we didn't consider $CeIr_5$ as the decomposition phase in this work. Meanwhile, among the possible $CeIr_2$, $CeIr_3$ and $FeIr_3$ binary phases, the formation enthalpy of $FeIr_3$ is substantially higher than that in $CeIr_2$ or $CeIr_3$. So, we choose $CeIr_2$ and $CeIr_3$ to assess the decomposition of $Ce_2Fe_{15}Ir_2$, which are described by the following formulas:

$$Ce_2Fe_{15}Ir_2 \rightarrow x_1CeIr_2 + x_2Ce + x_3Fe, \quad (1)$$

$$Ce_2Fe_{15}Ir_2 \rightarrow x_1CeIr_3 + x_2Ce + x_3Fe, \quad (2)$$

where the coefficients $x_i$ are subject to the stoichiometry constraint. The calculated decomposition enthalpies of $Ce_2Fe_{15}Ir_2$ are 0.082 eV/atom in formula (1) and 0.045 eV/atom in formula (2). It should be noted that, the "metastable" $CeFe_2$ is destined to decompose into

the "stable" $CeFe_5$ and Ce in the Materials Project database, which is in disagreement with experiment.[52,53] Moreover, $CeFe_2$ and $CeIr_2$ have the same $MgCu_2$-type crystal structure and in the ternary system, almost certainly, form a continuous solid solution. Therefore, we also estimate the possible decomposition as follows:

$$Ce_2Fe_{15}Ir_2 \rightarrow x_1CeIr_2 + x_2CeFe_2 + x_3Fe, \quad (3)$$

and the calculated decomposition enthalpy of $Ce_2Fe_{15}Ir_2$ is 0.096 eV/atom. While the positive nature of these decomposition enthalpies suggests a possibility of decomposition, we note that in previous experiments, many half-Heusler compounds[54] with the decomposition enthalpies of 0~100 meV/atom form successfully, as well as related rare-earth compounds in Table II. There is therefore a significant possibility that this material will form, particularly if non-equilibrium techniques such as a high-temperature quench are employed, where entropic stabilization becomes feasible.

In this work, the uniaxial magnetocrystalline anisotropy of Ir-substituted $Ce_2Fe_{17}$ is investigated only in the configuration of $Ce_2Fe_{15}Ir_2$. The magnetic properties of Ir-substituted $Ce_2Fe_{17}$ with different configurations require further study. Meanwhile, the increased price due to atom substitutions, especially the Ir compound, should be noted in later studies and industry application. Please also note that comparably expensive permanent magnet materials,[55] such as CoPt, have been produced and marketed, and are in fact extensively used in media such as hard disk drive platters.

# IV. CONCLUSION

In summary, through the first-principles calculations, the magnetic properties are investigated in 18*h*-site-substitued $Ce_2Fe_{14}M_3$ (*M*=Zn, Ga, Ge, As or Se) and 6*c*-site-substitued $Ce_2Fe_{15}W_2$ or $Ce_2Fe_{15}Ir_2$, for exploring the critical-element-free permanent

magnets. We find that the planar magnetocrystalline anisotropy in the 2-17 magnet $Ce_2Fe_{17}$ can be altered to the desired uniaxial behavior by atom substitutions. Among these investigated compounds, the uniaxial magnetocrystalline anisotropy is successfully induced in the 6*c*-site-substitued $Ce_2Fe_{15}Ir_2$ system. Meanwhile, $Ce_2Fe_{15}Ir_2$ retains the feature of strong magnetization in $R_2Fe_{17}$. In particular, $Ce_2Fe_{15}Ir_2$ shows an ultrahigh MAE of 11.25 $MJ/m^3$, which is comparable to most of the current rare earth permanent magnets. These results demonstrate the potential of atom substitutions in $Ce_2Fe_{17}$ for yielding critical-element-free permanent magnets.

# ACKNOWLEDGEMENTS

This research was supported by the Critical Materials Institute, an Energy Innovation Hub funded by the U.S. Department of Energy (DOE), Office of Energy Efficiency and Renewable Energy, Advanced Manufacturing Office. This research used resources of the Compute and Data Environment for Science (CADES) at the Oak Ridge National Laboratory (ORNL), which is supported by the Office of Science of the U.S. Department of Energy under contract No. DE-AC05-00OR22725. The Department of Energy will provide public access to these results of federally sponsored research in accordance with the DOE Public Access Plan.

# DATA AVAILABILITY

The data that support the findings of this study are available from the corresponding author upon reasonable request.

# REFERENCES


[1]J. M. D. Coey, Scr. Mater. **67,** 524 (2012).

[2]J. Marx, A. Schreiber, P. Zapp, and F. Walachowicz, ACS Sustain. Chem. Eng. **6,** 5858 (2018).

[3]A. Alam and D. D. Johnson, Phys. Rev. B **89,** 235126 (2014).

[4]H. İ. Sözen, S. Ener, F. Maccari, K. P. Skokov, O. Gutfleisch, F. Körmann, J. Neugebauer, and T. Hickel, Phys. Rev. Mater. **3,** 084407 (2019).

[5]Y. Makihara, Y. Uwatoko, H. Matsuoka, M. Kosaka, H. Fukuda, and H. Fujii, J. Magn. Magn. Mater. **272-276,** 551 (2004).

[6]I. Medvedeva, Z. Arnold, A. Kuchin, and J. Kamarád, J. Appl. Phys. **86,** 6295 (1999).

[7]D. P. Middleton, S. R. Mishra, G. J. Long, O. A. Pringle, Z. Hu, W. B. Yelon, F. Grandjean, and K. H. J. Buschow, J. Appl. Phys. **78,** 5568 (1995).

[8]X. C. Kou, F. R. de Boer, R. Grössinger, G. Wiesinger, H. Suzuki, H. Kitazawa, T. Takamasu, and G. Kido, J. Magn. Magn. Mater. **177-181,** 1002 (1998).

[9]H. Sun, J. M. D. Coey, Y. Otani, and D. P. F. Hurley, J. Phys.: Condens. Matter **2,** 6465 (1990).

[10]H. Sun, Y. Otani, and J. M. D. Coey, J. Magn. Magn. Mater. **104-107,** 1439 (1992).

[11]Z. h. Cheng, B. g. Shen, B. Liang, J. x. Zhang, F. w. Wang, S. y. Zhang, J. g. Zhao, and W. s. Zhan, J. Appl. Phys. **78,** 1385 (1995).

[12]S.-Q. Hao, N.-X. Chen, and J. Shen, Model. Simul. Mat. Sci. Eng. **10,** 425 (2002).

[13]K. V. S. Rama Rao, H. Ehrenberg, G. Markandeyulu, U. V. Varadaraju, M. Venkatesan, K. G. Suresh, V. S. Murthy, P. C. Schmidt, and H. Fuess, Phys. Stat. Sol. **189,** 373 (2002).

[14]T. Pandey, M.-H. Du, and D. S. Parker, Phys. Rev. Appl. **9** (2018).

[15]M. Artigas, D. Fruchart, O. Isnard, S. Miraglia, and J. L. Soubeyroux, J. Alloys Compd. **270,** 28 (1998).

[16]A. V. Andreev, J. Alloys Compd. **475,** 13 (2009).

[17]A. V. Andreev, S. Yoshii, M. D. Kuz'min, F. R. de Boer, K. Kindo, and M. Hagiwara, J. Phys.: Condens. Matter **21,** 146005 (2009).

[18]E. Girt and Z. Altounian, J. Appl. Phys. **87,** 4747 (2000).

[19]E. Girt and Z. Altounian, Phys. Rev. B **57,** 5711 (1998).

[20]Y. Janssen, S. Chang, A. Kreyssig, A. Kracher, Y. Mozharivskyj, S. Misra, and P. C. Canfield, Phys. Rev. B **76,** 054420 (2007).

[21]C. Du, H. Wang, F. Yang, and P. C. Hammel, Phys. Rev. B **90,** 140407 (2014).

[22]D. D. Sarma, Proceedings of the Indian Academy of Sciences - Chemical Sciences **90,** 19 (1981).

[23]H. L. Wang, C. H. Du, Y. Pu, R. Adur, P. C. Hammel, and F. Y. Yang, Phys. Rev. Lett. **112,** 197201 (2014).

[24]K. Yamauchi, P. Barone, T. Shishidou, T. Oguchi, and S. Picozzi, Phys. Rev. Lett. **115,** 037602 (2015).

[25]L. Yin, X. Wang, and W. Mi, ACS Appl. Mater. Interfaces **10,** 3822 (2018).

[26]G. Kresse and J. Furthmüller, Comput. Mater. Sci. **6,** 15 (1996).

[27]G. Kresse and J. Furthmüller, Phys. Rev. B **54,** 11169 (1996).

[28]P. Blaha, K. Schwarz, G. K. H. Madsen, D. Kvasnicka, and J. Luitz, WIEN2K, An augmented plane wave + local orbitals program for calculating crystal properties (Technische

Universität Wien, Vienna, 2001).

[29]E. Sjöstedt, L. Nordström, and D. J. Singh, Solid State Commun. **114,** 15 (2000).

[30]J. P. Perdew, K. Burke, and M. Ernzerhof, Phys. Rev. Lett. **77,** 3865 (1996).

[31]P. E. Blöchl, Phys. Rev. B **50,** 17953 (1994).

[32]G. Kresse and D. Joubert, Phys. Rev. B **59,** 1758 (1999).

[33]P. A. Teplykh, A. N. Pirogov, A. G. Kuchin, and A. E. Teplykh, Physica B: Condensed Matter **350,** E99 (2004).

[34]K. Momma and F. Izumi, J. Appl. Crystallogr. **44,** 1272 (2011).

[35]D. J. Singh and L. Nordstrom, Planewaves pseudopotentials and the LAPW method, 2nd ed. (Springer, Berlin, 2006).

[36]A. V. Andreev, D. Rafaja, J. Kamarad, Z. Arnold, Y. Homma, and Y. Shiokawa, J. Alloys Compd. **361,** 48 (2003).

[37]S. A. Nikitin, I. S. Tereshina, N. Y. Pankratov, E. A. Tereshina, Y. V. Skourski, K. P. Skokov, and Y. G. Pastushenkov, Phys. Solid State **43,** 1720 (2001).

[38]D. Vandormael, F. Grandjean, V. Briois, D. P. Middleton, K. H. J. Buschow, and G. J. Long, Phys. Rev. B **56,** 6100 (1997).

[39]S. Boseggia, R. Springell, H. C. Walker, A. T. Boothroyd, D. Prabhakaran, D. Wermeille, L. Bouchenoire, S. P. Collins, and D. F. McMorrow, Phys. Rev. B **85,** 184432 (2012).

[40]S. K. Panda, S. Bhowal, A. Delin, O. Eriksson, and I. Dasgupta, Phys. Rev. B **89,** 155102 (2014).

[41]H. Luo, Z. Hu, W. B. Yelon, S. R. Mishra, G. J. Long, O. A. Pringle, D. P. Middleton, and K. H. J. Buschow, J. Appl. Phys. **79,** 6318 (1996).

[42]H. Yamauchi, M. Yamada, Y. Yamaguchi, H. Yamamoto, S. Hirosawa, and M. Sagawa, J. Magn. Magn. Mater. **54,** 575 (1986).

[43]L. Ke, D. A. Kukusta, and D. D. Johnson, Phys. Rev. B **94,** 144429 (2016).

[44]J. Kudrnovský, I. Turek, V. Drchal, F. Máca, P. Weinberger, and P. Bruno, Phys. Rev. B **69,** 115208 (2004).

[45]F. Máca, J. Kudrnovský, V. Drchal, and G. Bouzerar, Appl. Phys. Lett. **92,** 212503 (2008).

[46]F. Pourarian, R. T. Obermyer, and S. G. Sankar, J. Appl. Phys. **75,** 6262 (1994).

[47]A. Jain, S. P. Ong, G. Hautier, W. Chen, W. D. Richards, S. Dacek, S. Cholia, D. Gunter, D. Skinner, G. Ceder, and K. A. Persson, APL Mater. **1,** 011002 (2013).

[48]A. Jain, G. Hautier, S. P. Ong, C. J. Moore, C. C. Fischer, K. A. Persson, and G. Ceder, Phys. Rev. B **84,** 045115 (2011).

[49]S. P. Ong, L. Wang, B. Kang, and G. Ceder, Chem. Mater. **20,** 1798 (2008).

[50]A. R. Akbarzadeh, V. Ozoliņš, and C. Wolverton, Adv. Mater. **19,** 3233 (2007).

[51]Y. Wang, Y. Zhang, and C. Wolverton, Phys. Rev. B **88,** 024119 (2013).

[52]K. H. J. Buschow and J. S. van Wieringen, Phys. Stat. Sol. (B) **42,** 231 (1970).

[53]K. Nassau, L. V. Cherry, and W. E. Wallace, J. Phys. Chem. Solids **16,** 123 (1960).

[54]J. Ma, V. I. Hegde, K. Munira, Y. Xie, S. Keshavarz, D. T. Mildebrath, C. Wolverton, A. W. Ghosh, and W. H. Butler, Phys. Rev. B **95,** 024411 (2017).

[55]C. Tannous, Comstock, R. L. Magnetic information-storage materials. in: Kasap S., Capper P. (eds) springer handbook of electronic and photonic materials, (2017).

# TABLE NOTES

TABLE I. The lattice constants, volumes, total magnetic moments $m_{tot}$ (spin plus orbital moments), atomic spin and orbital moments in fully relaxed $Ce_2Fe_{17}$ and $Ce_2Fe_{15}Ir_2$. The atom labels correspond to Fig. 1.

| | $Ce_2Fe_{17}$ | $Ce_2Fe_{15}Ir_2$ |
|---|---|---|
| $a=b$ (Å) | 8.445 | 8.440 |
| $c$ (Å) | 12.610 | 12.834 |
| $\alpha=\beta$ (°) | 90.00 | 90.00 |
| $\gamma$ (°) | 120.00 | 120.00 |
| Volume (Å$^3$) | 778.885 | 791.707 |
| $m_{tot}$ ($\mu_B$/f.u.) | 38.249 | 35.080 |
| $\mu_{Ce}^{spin}$ / $\mu_{Ce}^{orbit}$ ($\mu_B$) | -0.726/0.236 | -0.668/0.181 |
| $\mu_{Fe\text{-}6c}^{spin}$ / $\mu_{Fe\text{-}6c}^{orbit}$ ($\mu_B$) | 2.654/0.045 | — |
| $\mu_{Fe\text{-}9d}^{spin}$ / $\mu_{Fe\text{-}9d}^{orbit}$ ($\mu_B$) | 2.140/0.034 | 2.186/0.080 |
| $\mu_{Fe\text{-}18f}^{spin}$ / $\mu_{Fe\text{-}18f}^{orbit}$ ($\mu_B$) | 2.463/0.042 | 2.516/0.067 |
| $\mu_{Fe\text{-}18h}^{spin}$ / $\mu_{Fe\text{-}18h}^{orbit}$ ($\mu_B$) | 2.286/0.044 | 2.317/0.057 |
| $\mu_{Ir\text{-}6c}^{spin}$ / $\mu_{Ir\text{-}6c}^{orbit}$ ($\mu_B$) | — | 0.442/0.019 |

TABLE II. The enthalpies of formation ($\triangle H_f$), decompositions and related decomposition enthalpies ($\triangle H_d$) of $R_2Fe_{17}$ and compounds with Ce, Fe or Ir atoms in Materials Project data base.

| Compounds | $\triangle H_f$ (eV/atom) | Decompose to | $\triangle H_d$ (eV/atom) |
|---|---|---|---|
| $Ce_2Fe_{15}Ir_2$ | -0.042 | discussed | discussed |
| $CeFe_5$ | -0.009 | Stable | — |
| $CeFe_2$ | 0.031 | $CeFe_5$+Ce | 0.038 |
| $CeIr_2$ | -0.795 | Stable | — |
| $CeIr_3$ | -0.634 | Stable | — |
| $CeIr_5$ | -0.366 | $CeIr_3$+Ir | 0.056 |
| $FeIr_3$ | -0.073 | Stable | — |
| Ce | 0.002 | Stable | — |
| Fe | 0.000 | Stable | — |
| Ir | 0.000 | Stable | — |
| $Ce_2Fe_{17}$ | 0.015 | $CeFe_5$+Fe | 0.021 |
| $Pr_2Fe_{17}$ | 0.054 | Pr+Fe | 0.054 |
| $Nd_2Fe_{17}$ | 0.322 | Nd+Fe | 0.322 |
| $Sm_2Fe_{17}$ | 0.297 | Sm+Fe | 0.297 |

# FIGURE CAPTIONS

**FIG. 1.** The geometries of $Ce_2Fe_{17}$, $Ce_2Fe_{14}M_3$ (*M*=Zn, Ga, Ge, As or Se), $Ce_2W_2Fe_{15}$ and $Ce_2Ir_2Fe_{15}$. The newly introduced *M* atoms in $Ce_2Fe_{17}$ occupy the 18*h* site. The W or Ir atom occupies the 6*c* sites.

**FIG. 2.** The calculated MAE in $Ce_2Fe_{17}$ with different (a) ***k*** points and (b) Hubbard U values of Ce *f* electrons. (c) The total and Ce-*f*-decomposed density of states (DOS) in $Ce_2Fe_{17}$ at $U_{Ce,f}$=0 and 2 eV respectively. The solid lines in (c) correspond to the $U_{Ce,f}$=0 eV case, and the dashed lines represent the $U_{Ce,f}$=2 eV case. The positive and negative values in the vertical axis denote the spin-up and spin-down channels, respectively. The Fermi level is 0 eV. (d) The calculated MAE in $Ce_2Fe_{14}Si_3$ with different substitutions of Fe by Co.

**FIG. 3.** (a) The total energies of $Ce_2Fe_{15}M_2$ (*M*=Zn or Ga), $Ce_2Fe_{15}W_2$ and $Ce_2Fe_{15}Ir_2$ systems as the newly introduced atoms lie in 6*c*, 9*d*, 18*f* and 18*h* sites respectively. The calculated (b) volumes, (c) MAE and (d) magnetization in $Ce_2Fe_{17}$, $Ce_2Fe_{14}M_3$ (*M*=Zn, Ga, Ge, As or Se) and $Ce_2Fe_{15}Ir_2$ systems with GGA+SOC. The error bars of $Ce_2Fe_{17}$ and $Ce_2Fe_{15}Ir_2$ systems in Fig. 3(c) represent the MAE standard deviations of 0.025 MJ/m$^3$ and 0.047 MJ/m$^3$ respectively, which are calculated based on the 2000, 3000, 4000 and 5000 **k** points.

**FIG. 4.** The (a) total DOS and (b) *d*-orbital DOS for Ir atom in $Ce_2Fe_{15}Ir_2$. The partial DOS

projected on the *d* states for Ir atom in $Ce_2Fe_{15}Ir_2$ are shown in (b), where the red, blue and magenta solid lines denote the contributions from $m$=0 ($d_{z^2}$), $m$=±1 ($d_{xz}$ and $d_{yz}$) and $m$=±2 ($d_{xy}$ and $d_{x^2-y^2}$) states respectively. The positive (negative) values in the vertical axis denote the spin-up (spin-down) channel. The gray area in (a) denotes the total DOS of $Ce_2Fe_{17}$. The Fermi level is 0 eV.

**FIG. 5.** (a-c) Three kinds of ferrimagnetic orders considered in $Ce_2Fe_{17}$. The magnetic order of the dashed-line-marked zones in (a-c) are shown in (d). (e) The calculated Curie point in $Ce_2Fe_{17}$ based on the FI-order1, FI-order2 and FI-order3 respectively.

**FIG.** 1, L. Yin *et al.*

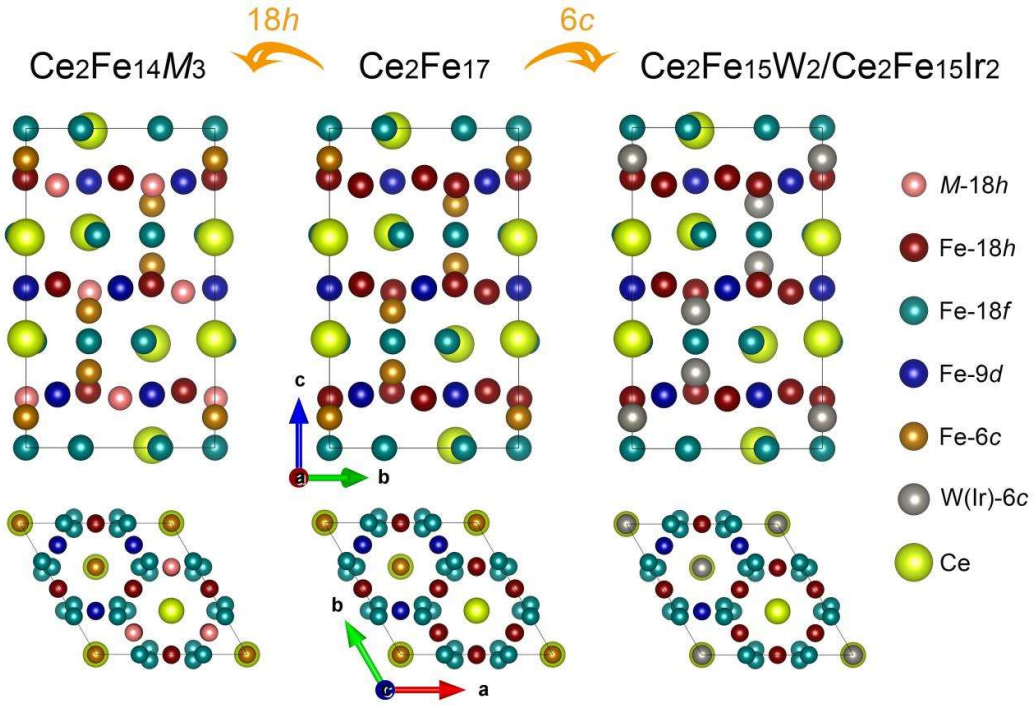

**FIG.** 2, L. Yin *et al.*

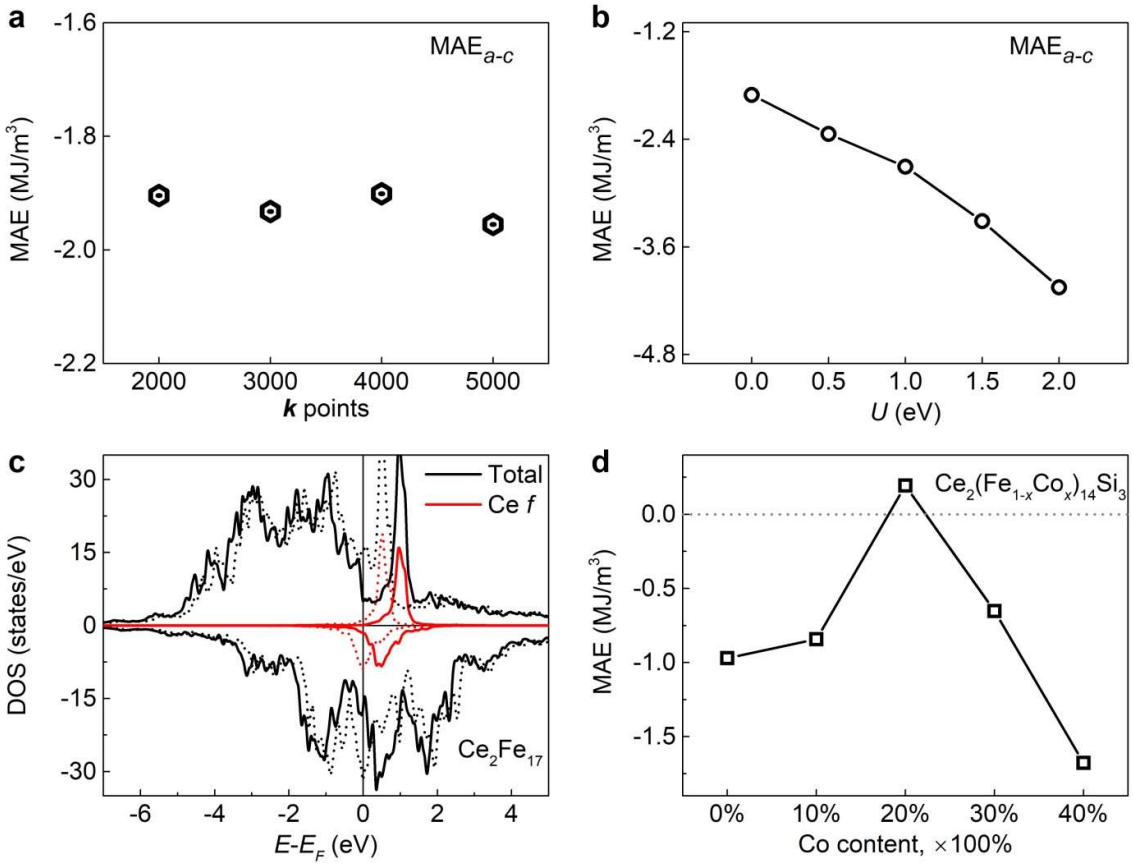

**FIG.** 3, L. Yin *et al.*

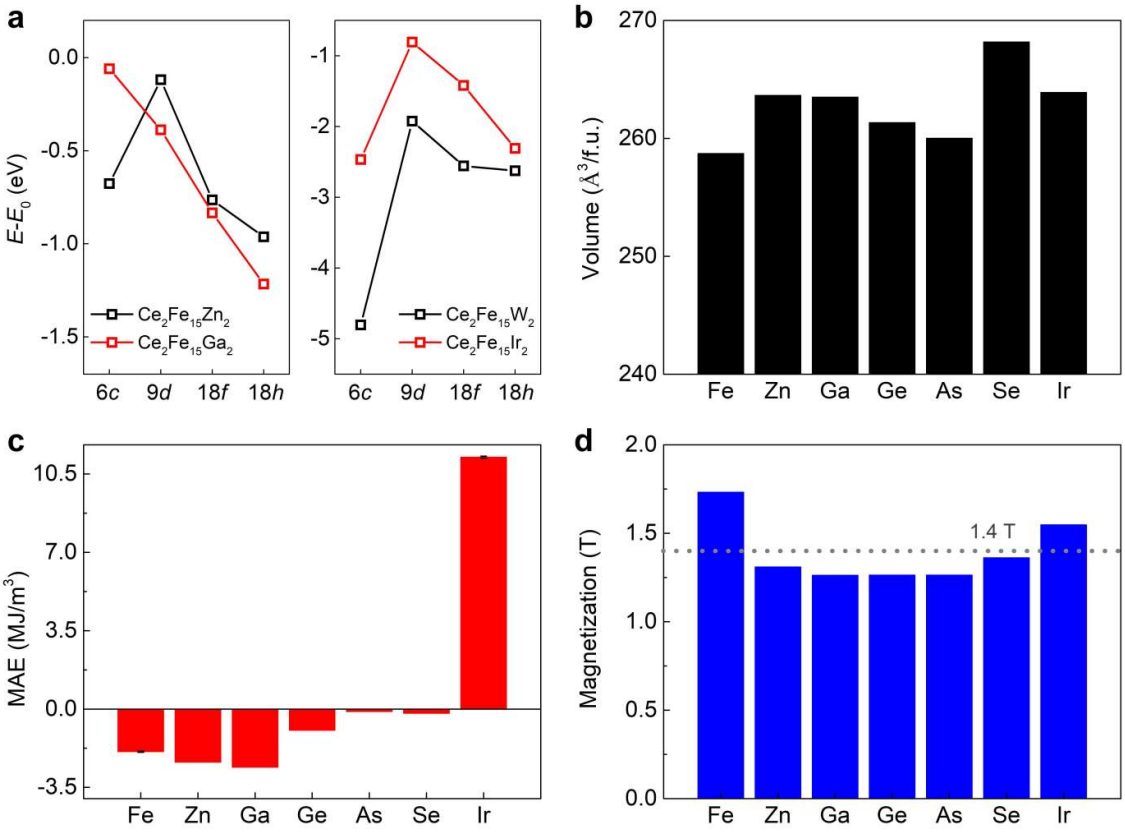

**FIG.** 4, L. Yin *et al.*

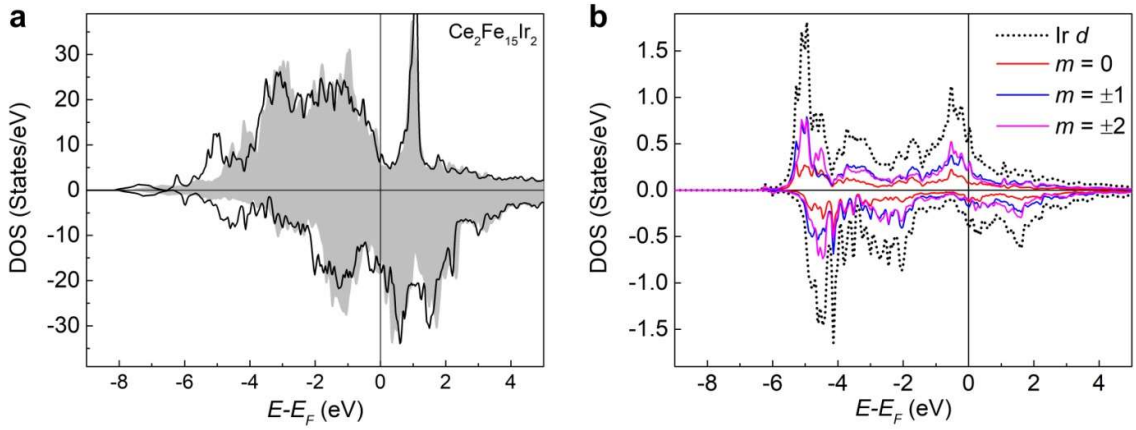

**FIG.** 5, L. Yin *et al.*